Biomaterials xxx (2013) 1–9

Contents lists available at ScienceDirect

Biomaterials

journal homepage: www.elsevier.com/locate/biomaterials

A pH-responsive hybrid fluorescent nanoprober for real time cell labeling and endocytosis tracking

Shu Chang [a, 1], Xumeng Wu [b, 1], Yongsheng Li [a, *], Dechao Niu [a], Yongping Gao [a], Zhi Ma [c], Jinlou Gu [a], Wenru Zhao [a], Weihong Zhu [b, *], He Tian [b], Jianlin Shi [a, d, **]

[a] Lab of Low-Dimensional Materials Chemistry, Key Laboratory for Ultrafine Materials of Ministry of Education, School of Materials Science and Engineering, East China University of Science and Technology, Shanghai 200237, China
[b] Shanghai Key Laboratory of Functional Materials Chemistry, Key Laboratory for Advanced Materials and Institute of Fine Chemicals, East China University of Science & Technology, Shanghai 200237, China
[c] Shanghai Institute of Organic Chemistry, Chinese Academy of Sciences, Shanghai 200032, China
[d] Shanghai Institute of Ceramics, Chinese Academy of Sciences, Shanghai 200050, China

ARTICLE INFO

Article history:
Received 31 July 2013
Accepted 13 September 2013
Available online xxx

Keywords:
Copolymer
Self assembly
Nanoparticle
Fluorescence
Biosensor
Image analysis

ABSTRACT

Hydrophilic, fluorescent hybrid nanoprobes (NDI@HNPs) encapsulated with the hydrophobic pH-responsive fluorophore (*N,N′*-di-*n*-dodecyl-2,6-di(4-methyl-piperazin-1-yl)naphthalene-1,4,5,8-tetracarboxylic acid diimide, NDI) for recognizing and mapping the route of cell phagocytosis have been fabricated based on the self-assembly of amphiphilic diblock copolymer PS-*b*-PAA and the subsequent shell cross-linking with 3-mercaptopropyltrimethoxy silane (MPTMS). The as-synthesized NDI@HNPs has a typical spherical morphology of 46 nm in diameter with excellent monodispersity in aqueous solution. The NDI@HNPs probe exhibits extremely low cytotoxicity, fast real time pH response and enhanced fluorescence intensity under acidic environment with respect to the corresponding free dye in highly polar aqueous system because of the encapsulation of NDI molecules inside nanoparticle cores with weak polarity environment. The fluorescence intensity of NDI@HNPs is enhanced by 55-fold upon changing from neutral (pH = 7.4) or basic (pH = 8.4) to acid (pH = 3.4) in aqueous system, in contrast to the serious fluorescence quenching of free NDI in the same medium, which can exactly meet the physiological pH range in cells. The favorably long emission wavelength is beneficial to the low scattering and minimal interfering requirements to fluorescent bioimaging. Moreover, functionalization with rapid cell-penetrating peptides (HIV-1 TAT) allows them to overcome the physiological and biological barriers during the phagocytosis process. Its characteristic fluorescent response to pH benefits the intracellular labeling and organelle targeting, realizing the real time tracking of the probe entry into cancer cells, the accumulation into the endolysosome and the further escape.

1. Introduction

Understanding the intracellular environment and biological interactions at the sub-cellular level is an important research area of molecular cell biology and chemical biology. Modern optical microscopy allows the widespread applications of a variety of fluorescent molecular probes, such as fluorescent proteins, quantum dots, upconversion materials and molecular fluorophores in both *in vitro* and in vivo cellular imaging and sub-cellular detection [1–6]. Especially, smart bioimaging agents with specific responsive characters to some specific physiological environments such as ionic potentials, pH value or enzymatic expressions have become the new focuses on cellular signaling [7–14]. Intracellular pH plays an important role in all these stimuli since it could reveal the basic cell physiological processes including the metabolic acid production, leakage of acid across plasma, and organelles membranes and membrane transport processes [15–17]. Efforts on development of pH-responsive fluorescent bio-probes have been made in conjugating pH-responsive dyes with polymers to realize high biocompatibility, even in constructing a low-cost microbioreactor pH indicator for high-throughput bioprocessing [18–24].

* Corresponding authors.
** Corresponding author. Lab of Low-Dimensional Materials Chemistry, Key Laboratory for Ultrafine Materials of Ministry of Education, School of Materials Science and Engineering, East China University of Science and Technology, Shanghai 200237, China.
E-mail addresses: ysli@ecust.edu.cn (Y. Li), whzhu@ecust.edu.cn (W. Zhu), jlshi@mail.sic.ac.cn (J. Shi).
[1] S.C. and X.M.W. contributed equally to this work.

0142-9612/$ – see front matter © 2013 Elsevier Ltd. All rights reserved.
http://dx.doi.org/10.1016/j.biomaterials.2013.09.044

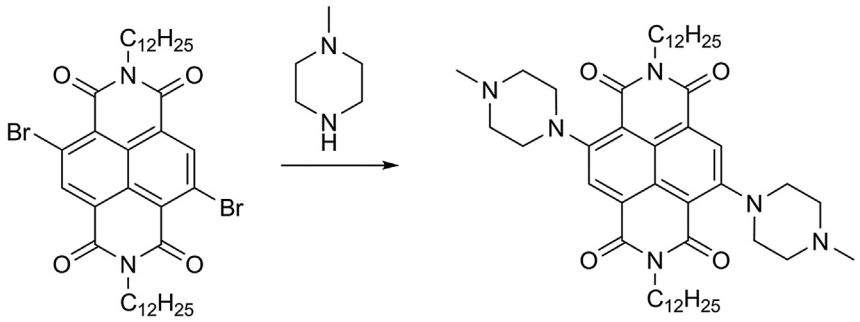

Scheme 1. Synthetic route of NDI.

Recently, the considerable nanoparticle (NP)-based hybrid systems derived from silica or siloxanes have been explored in the laboratory and clinical cancer therapies. The NPs can be prepared by the colloid methods, with uniform size and shape distributions, and ultra-fine colloidal stability in aqueous systems [25–32]. Furthermore, the unique properties of colloidal NPs can also be achieved by facile functionalization on the outer shells. Actually, the combination of fluorophores and colloidal NPs can overcome the limitations of conventional fluorescent probes such as organic dyes and fluorescent proteins [33–37]. Especially for biological applications, the fluorescent colloidal NPs demonstrate several advantages such as high quantum yield in the aqueous solution, enlarged Stokes shift, low cytotoxicity and the potential of environmental sensibility [38–40]. The cellular uptake of NPs is mainly governed by the clathrin-mediated endocytosis, which transfers the NPs into either endosomes (pH 5.0–6.0) or lysosomes (pH 4.0–5.0). For the acidic intracellular microenvironment detection of tumor cells, acidity-induced responding nature of fluorescent NPs should be highly sensitive in the pH range of 4.0–6.0 [20,41–43]. Meanwhile, the size distribution of NPs should be narrow enough to prevent the successive physiological and biological barriers from cell to organelles. Importantly, it is essential of the NP probe system to endow a highly biological stability to inhibit the degradation effect of the endolysomal acid and hydrolase [44–47].

To address the aforementioned issues, we designed and synthesized a pH-responsive fluorescent hybrid nanoprobes (NDI@HNPs) system for real time intracellular cancer cell imaging. The hydrophobic pH sensitive dye molecule, *N,N′*-di-*n*-dodecyl-2,6-di(4-methyl-piperazin-1-yl)naphthalene-1,4,5,8-tetracarboxylic acid diimide (NDI), is derived from the classical naphthalenediimide fluorophore. The *in situ* immobilization of NDI fluorophores into the spherical PS-*b*-PAA micelles forms pH-responsive nanoprobes in an aqueous system. Crucially, the low cross-linking density of MPTMS shells can guarantee the fast pH response of the encapsulated fluorophores, along with high biocompatibility and extremely low cytotoxicity. Facilitated with our unique strategy, the NDI@HNPs possesses several remarkable features in the intracellular imaging applications: (i) excellent water-solubility of NDI@HNPs due to the high hydrophilicity of the shell layer of the nanoparticles in spite of the high hydrophobicity of free dye NDI; (ii) sub-50 nm monodispersed hydrophilic nanoparticles obtained which have hydrolyzed MPTMS shells for preventing the dissociation or leakage of encapsulated fluorophores; (iii) distinctly decreasing fluorescence quenching of NDI in NDI@HNPs in aqueous system; (iv) fast and precise pH response (from pH 8.4 to 3.4, 55-fold enhancement in fluorescence) of the encapsulated fluorophores, along with extremely low cytotoxicity through the low cross-linking density of MPTMS shells; (v) easy functionalization with rapid cell-penetrating peptides (HIV-1 TAT) to overcome the physiological and biological barriers for routing the *in vitro* cancer cell phagocytosis pathway. The integration of remarkable pH-sensitivity, cancer intracellular environment detection and negligible cytotoxicity of the synthesized NDI@HNPs provides a valuable tool to the intracellular tumor cell labelinglabeling and organelle tracking.

2. Materials and methods

2.1. Materials

All reagents and solvents were purchased from commercial sources, and are of analytical grade. The preparation of *N,N′*-di-*n*-dodecyl-2,6-dibromonaphthalene-1,4,5,8-tetracarboxylic acid diimide (NDI, Scheme 1) was conducted according to literature methods [48]. The amphiphilic block copolymer, PS_{95}-*b*-PAA_{25} was prepared by the sequential atomic transfer radical polymerization (ATRP) method reported by Kang et al. [49].

^1H and ^{13}C NMR in $CDCl_3$ or [D_6]DMSO were recorded on a Bruker Avance-400 spectrometer with tetramethylsilane (TMS) as the internal standard. Data for ^1H NMR spectra are reported as follows: chemical shift (ppm) and multiplicity (s = singlet, d = doublet, t = triplet, q = quartet, m = multiplet). Data for ^{13}C NMR spectra are reported in ppm. HRMS were measured on a Waters LCT Premier XE spectrometer. UV/Vis spectra were obtained by using a Varian Cary 500 spectrophotometer (1 cm quartz cell) at 25 °C. Fluorescence spectra were recorded on a Varian Cary Eclipse fluorescence spectrophotometer (1 cm quartz cell) at 25 °C. The slit width was 5 nm for both excitation and emission. Flash chromatography was conducted by using silica-gel column packages purchased from Qingdao Haiyang Chemical Co. (China).

2.2. Preparation of N,N′-di-n-dodecyl-2,6-di(4-methyl-piperazin-1-yl)-1,4,5,8-tetracarboxylic acid diimide (NDI)

The mixture of NDI-Br (160 mg, 0.2 mmol) and *N*-methyl piperazine (5 mL) was stirred at room temperature overnight under an argon atmosphere. After removing the excess of *N*-methyl piperazine in vacuo, the residue was dissolved in an aqueous solution of 0.1 M HCl (50 mL) and extracted with dichloromethane (3 × 40 mL). The combined organic layer was washed with saturated brine, dried over anhydrous $MgSO_4$, filtered and rotary evaporated. The crude product was purified by silica-gel chromatography by using methanol/dichloromethane 1:20 as the elute to afford a deep purple solid (40 mg, 24% yield). ^1H NMR (400 MHz, $CDCl_3$, ppm): δ 8.441 (s, 2H, Ph-H), 4.164 (*t*, 4H, N–CH_2–), 3.466 (s, 8H, piperazine-H), 2.760 (s, 8H, peperazine-H), 1.702 (m, 4H, *N*–CH_2–CH_2), 1.200–1.460 (m, 36H, –CH_2), 0.875 (*t*, 6H, –CH_3). ^{13}C NMR (100 MHz, $CDCl_3$, ppm): δ 162.914, 161.872, 151.833, 125.790, 125.014, 124.657, 110.155, 55.014, 52.100, 45.980, 40.901, 31.914, 29.967, 29.637, 29.625, 29.584, 29.354, 28.186, 27.164, 22.685, 14.128. Mass spectrometry (ESI-MS, *m*/*z*): $[M + H]^+$ calcd for $C_{48}H_{75}N_6O_4$, 799.5850; found, 799.5854.

2.3. Synthesis of hybrid nanoprobes NDI@HNPs

0.015 g of PS_{95}-*b*-PAA_{25} and 5 mg NDI were dissolved in 10 mL of DMF in a glass beaker and vigorously stirred in room temperature to become a homogenous solution. 40 mL ultra-pure water was poured into the dye-contained solution under vigorous stirring. The resulted transparent dark purple solution contained the core–shell structured micelles generated by block copolymers with immobilized NDI. The organic silane 3-mercaptopropyltrimethoxy-silane (MPTMS) was introduced into the system as a stabilizer to further improve the confinement of NDI dyes. The cross-linked shell was prepared by adding 2 mL of ethanol solution of 50 mg MPTMS dropwise in the presence of 1 mL NH_3, and continued for 6 h. Both DMF and NH_3 were eliminated by dialysis for one day. A transparent purple suspension was obtained.

Please cite this article in press as: Chang S, et al., A pH-responsive hybrid fluorescent nanoprober for real time cell labeling and endocytosis tracking, Biomaterials (2013), http://dx.doi.org/10.1016/j.biomaterials.2013.09.044

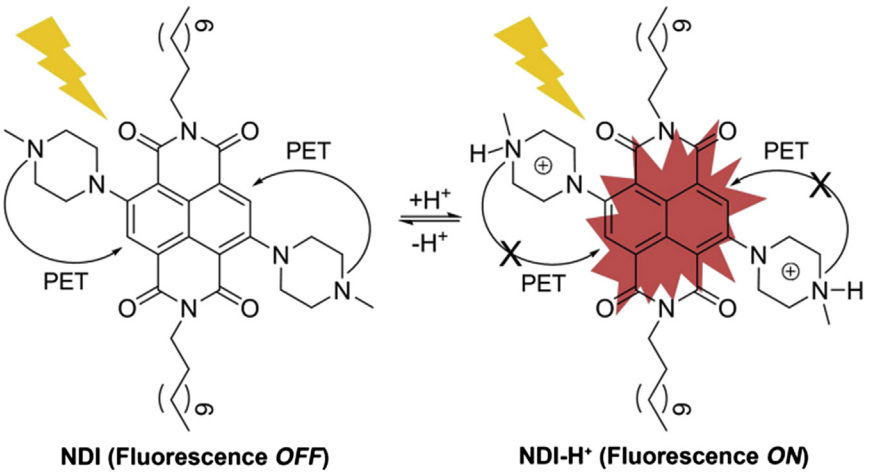

Scheme 2. pH response of NDI based on PET mechanism which can be blocked by the protonation of piperazines.

The product was collected by centrifugation at 4000 rpm/min for 10 min for 3 times by the Amicon Ultra-15 Centrifugal Filters (Millipore, USA), and freeze-dried in vacuum for 24 h. The encapsulated efficiency was calculated by the UV–Vis absorbance of the as-prepared nanoparticles. The weight percentage of cyanine dye was about 5%, chosen as the practical proportion without further optimization.

2.4. Synthesis of TAT-conjugated NDI@HNPs

The HIV-1 TAT peptides were purchased from the Chinese Peptides Company. The high cell membrane penetrated peptide HIV-1 TAT peptides were conjugated onto the outer surface of NDI@HNPs through the amide bonding between the residual carboxyl groups of PAA blocks and the amino groups of TAT peptides by employing the cross-linking reagents EDC and NHS. The 5 mg TAT was dissolved in 2.5 mL phosphate buffered saline (PBS) solution to get a TAT stocked solution. The NDI@HNPs were collected by centrifugation, and re-suspended in 20 mL PBS solution. The −COOH groups of the PAA branches were activated by 200 mg EDC with 50 mg NHS, stirring at room temperature for 12 h. Subsequently, the TAT-contained solution was added into the above solution, and the mixture solution was kept stirring for additional 12 h. The TAT-conjugated nanoparticles were collected by centrifugation at 20,000 rpm/min for 20 min at 4 °C.

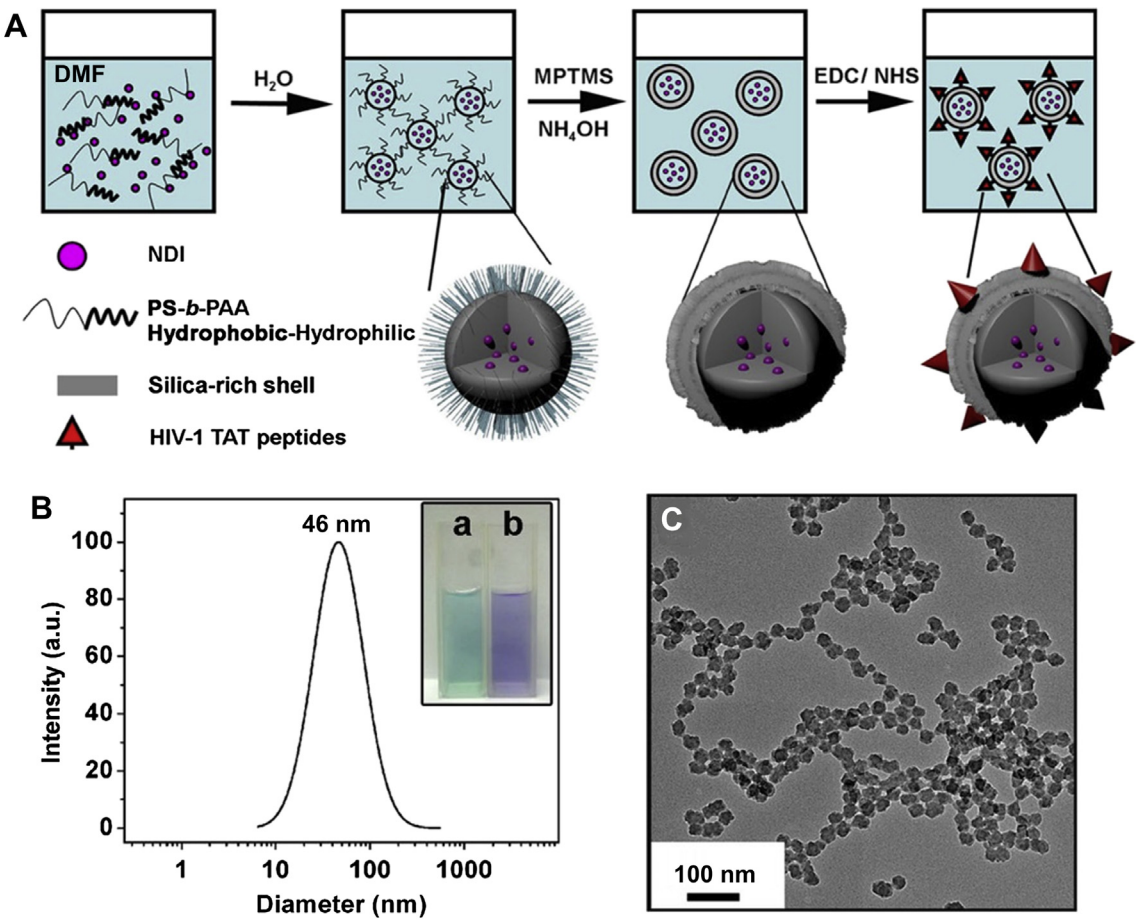

Fig. 1. (A) Schematic diagram of synthetic strategy of colloidal pH-responsive fluorescent hybrid nanoprobes NDI@HNPs. (B) Dynamic-diameter distribution curve of NDI@HNPs obtained by DLS, with average diameter of 46 nm. Inset: photographic image of NDI@HNPs suspended in aqueous medium at pH 8.4 (a) and pH 4.4 (b). (C) TEM image of the as-synthesized NDI@HNPs.

Please cite this article in press as: Chang S, et al., A pH-responsive hybrid fluorescent nanoprober for real time cell labeling and endocytosis tracking, Biomaterials (2013), http://dx.doi.org/10.1016/j.biomaterials.2013.09.044

2.5. Morphology characterization

The size distribution of HNPs was evaluated by dynamic light scattering (DLS) by a Nicomp TM 380 ZLS zeta-potential/particle sizer (PSS Nicomp particle size system, USA). Transmission electron microscopy (TEM) was employed for morphology characterization on a JEM 2100F electron microscope operated at 200 KV.

2.6. Spectroscopic measurement and acidic constant calculation

The time-course fluorescence measurement was operated on a HORIBA FluoroMax-4 spectrofluorometer (1 cm quartz cell) at 25 °C. The UV–Vis absorption spectra were performed by a Shimadzu 2550 spectroscope, while the Photoluminescent spectra were collected by a Shimadzu RF5301pc. The acidity constant (pK_a) value of NDI@HNPs in water was calculated based on Henderson-Hasselbalch treatment (eq. (1)) according to the fluorometric titration.

$$\log[(I_{Fmax} - I_F)/(I_F - I_{Fmin})] = pH - pK_a \quad (1)$$

Here, I_F corresponds to the fluorescent intensity of NDI@HNPs.

2.7. In vitro cytotoxicity test, apoptosis analysis, flow cytometry and CLSM observation

We employed the Human Breast cancer MCF-7 cells for testing the cell viability by the MTT (3-(4,5-Dimethylthiazol-2-yl)-2,5-diphenyltetrazolium bromide) method. The cells were cultivated at 37 °C in DMEM with 10% FCS. For the cytotoxicity test, the cells were seeded in a 96-well plate at a density of 8000–10 000 cells per well, and grown for 24 h at 37 °C, 5% CO_2 and 95% humidity. Then, freeze-dried NDI@HNPs were dispersed into the medium with concentrations of 65, 125, 250, 500, 1000 μg mL^{-1}, respectively. After one-day incubation, 5 mg mL^{-1} 3-[4,5-dimethylthiazol-2-yl]-2,5-diphenyltetrazolium bromide (MTT) was dissolved in DMEM (Dulbecco's Modified Eagle's Medium) with 10% FCS, and incubated for 3.5–4 h, followed by adding DMSO into each well. Absorption was measured on a microplate reader (ELx800, Bio-Tek) at 490 nm.

To evaluate the cell imaging ability, MCF-7 cells were seeded in a 1.5 inches imaging plate with an amount of 30,000 cells mL^{-1}. The TAT-NDI@HNPs were co-cultivated with MCF-7 cells for 1, 4, 8, 20 h at 37%, 5% CO_2 and 95% humidity. Before the confocal laser scanning microscopy (FluoView FV1000, Olympus) observation, the cells were washed 3 times with PBS (pH = 7.4). First, the pre-warmed 50 nM stock solution of LysoTacker was added into the dish and incubated with the cells for 30 min at 37 °C. Then, the cells were fixed by 4% paraformaldehyde for 10 min at 4 °C and washed twice with PBS. 0.5 mL of Hoechst 33258 solution in ultra-pure water was added, and incubated for 5 min to stain the nuclei, followed by softly washing twice to remove excessive dyes. Finally, 1 mL of PBS solution was added and the cells were visualized under a CLSM. The fluorescence images were taken under 60× oil-immersion objective. Blue, green and red luminescent emissions from Hoechst 33258, LysoTracker® Green DND-99 (Invitrogen) and TAT-NDI@HNPs were excited at the wavelength of 405, 450 and 560 nm, respectively. The emission wavelengths were ranged from 425 to 450 nm for Hoechst 33258, 600–650 nm for NDI@HNPs, and 505–525 nm for LysoTracker Green. The scanning mode was in sequential frame without any interference between 3 channels.

The flow cytometry was carried out by Becton Dickinson FACS Calibur (Becton Dickinson, San Jose, CA). The MCF-7 cells and the Human Liver L-02 cells were seeded in 6 cm dishes with a density of 10^5 cells per dish. The TAT-NDI@HNPs were co-cultivated with MCF-7 cells and the L-02 cells for 1, 4, 8 h at 37 °C, 5% CO_2 and 95% humidity. After the co-cultivation, the cells were removed by treatment with EDTA, washed with PBS, and collected by centrifugation at 1200 r/min for 5 min. The cells were washed for 3 times. At the end of the incubation period, the medium was removed, cells were washed with DMEM, trypsinized, and cell-associate fluorescence was quantified by BD FACS Calibur at Channel FL-3. The data analysis was performed using the CellQuest software (Becton Dickinson). The live cells were gated on the basis of forward and side scatter. A total of 10,000 events were acquired for each sample.

3. Results and discussion

3.1. Design and synthesis of NDI@HNPs

Naphthalene diimides are a versatile class of chromophores with a typical intramolecular charge transfer (ICT) character, showing the high tunability of their optical and electrochemical properties by functionalization of the parent naphthalene diimide core at the 2,3,6,7 positions. The introduction of electron-donating groups is a powerful tool to decrease the optical band gap of NDI chromophore through ICT mechanism and sequentially shift the fluorescence wavelength, even falling in the NIR range [50–52]. In the chromophore of NDI (Scheme 2), photo-induced electron transfer (PET) from the methyl-substituted nitrogen atoms to naphthalene diimide chromophore can quench the fluorescence which can be blocked by the protonation of them, resulting in the specific pH response from fluorescence OFF (NDI) to fluorescence ON (NDI-H^+) [53]. Additionally, the two hydrophobic dodecyl units at the imide sides benefit for the formation of micelles with the help of the diblock copolymer (Scheme 1 and Supporting Information: Figs. S1–S3). The 4-methyl-piperazine unit was incorporated onto the chromophore core to realize both the pH control of the PET process and an enhanced push–pull system with a long emission wavelength at 622 nm [53].

Our strategy to prepare the pH-responsive hybrid nanoprobes involves the encapsulation of pH-responsive fluorophore NDI into the spherical micelles of the PS-*b*-PAA, and further stabilization by the hydrolysis of organic silane MPTMS (Fig. 1A). Briefly, NDI and PS-*b*-PAA were firstly dissolved in 2,5-dimethylfuran to obtain a homogenous organic solution. Upon addition of water, the quick transformation of oil-to-water phase induced the formation of polymeric nanosized spherical micelles with a hydrophobic PS inner core and hydrophilic PAA outer arms. The hollow inner caves of the hydrophilic micelles could be employed to store hydrophobic NDI without the need of any chemical conjugation. After shell cross-linking via a silane coupling agent MPTMS, a kind of water-soluble pH-responsive fluorescent hybrid nanoprobes (NDI@HNPs) were fabricated. Obviously, the one-pot encapsulation strategy can avoid the complicated functionalization or pre-treatments such as the covalent bonding between fluorophores and skeleton units. Based on the standard absorption curves, the content of NDI dye immobilized into HNPs was calculated to be 0.09 mmol g^{-1} (Supporting Information: Fig. S4).

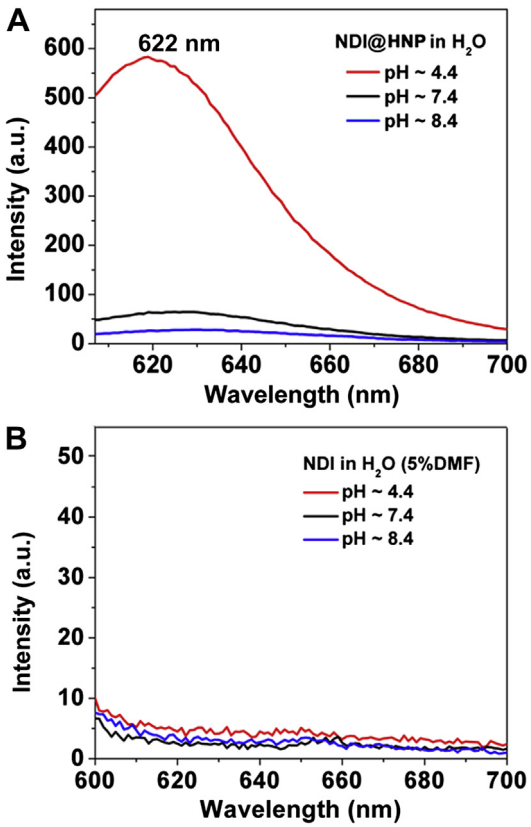

Fig. 2. Changes in fluorescence spectra in acidic (pH = 4.4), neutral (pH = 7.4) and basic (pH = 8.4) media: (A) NDI@HNPs in H_2O and (B) free NDI dye dispersed in H_2O containing 5% DMF.

Please cite this article in press as: Chang S, et al., A pH-responsive hybrid fluorescent nanoprober for real time cell labeling and endocytosis tracking, Biomaterials (2013), http://dx.doi.org/10.1016/j.biomaterials.2013.09.044

Since the encapsulated fluorophores in HNPs are aimed at pH response, the thickness of the outer silica-rich shell should be precisely controlled to allow the quick interchange of H^+ ions while maintains the well-protection of encapsulated dye molecules from leakage. Based on our previous work [53–55], the thickness of the silica shell was precisely adjusted by controlling the initial MPTMS amount and the reaction time. We optimized the consumption amount of MPTMS and the hydrolysis time duration (6 h), resulting in the thin silica-rich layers confirmed by the energy-dispersive X-ray spectroscopy (EDS). Finally, the carboxylic groups on PAA arms could be easily conjugated with the high cell-penetrating peptides, HIV-1 TAT, through the reaction of amide bonding (amidation) for increasing the cell-penetrating ability of NDI@HNPs.

3.2. Morphological characterization and stability of NDI@HNPs

Fig. 1B shows the size distribution of the as-prepared NDI@HNPs measured by Dynamic Light Scattering (DLS), indicative of a narrow size distribution around 46 nm, along with high water-solubility. The obtained NDI@HNPs suspended in aqueous system without aggregation or precipitation (the inset of Fig. 1B) [56,57]. Moreover, transmission electron microscopy (TEM) result also demonstrates that monodispersed hybrid nanoprobes were uniformly distributed in the field of view with a diameter of less than 40 nm (Fig. 1C). There was a subtle 6-nm discrepancy between the mean particle diameters obtained from the DLS result and TEM image, which could be attributed to the extension of PAA chains on the thin silica-rich shell. This result also gives indirect evidence that the cross-linking reaction of MPTMS is at around the PAA outer arms instead of on the surface of spherical micelles. Clearly, the particle size is small enough to effectively penetrate into tissues and through cytomembrance [58–62]. To further confirm the existence of the silica-rich shell, Energy-Dispersive X-ray Spectroscopy (EDS) spectrum was recorded on the shell region of the nanoparticle. Both of Si and S peaks could be clearly observed (Supporting Information: Fig. S5), indicative of the successful shell cross-linking with MPTMS. Besides, the external free groups of −SH and −COOH at PAA outer arms can endow the cross-linked nanoparticles with a negative zeta potential of −29 mV and the potential for further functionalization.

3.3. Optical properties of NDI@HNPs

First of all, the influence of low density cross-linking of silica shells on the pH-response performance of NDI@HNPs was investigated. Excitingly, upon changing pH from basic (8.4) or neutral (7.4) to acid (4.4) in aqueous solution of NDI@HNPs, the fluorescence of NDI@HNPs was significantly enhanced by 55-fold with a minor blue-shift (Fig. 2A), along with a solution color change from blue to purple (Fig. 1B inset and Fig. S6, Supporting Information). Fortunately, the precisely controlled cross-linking of the silica shells does not affect the pH response. Here the fluorescence enhancement of NDI@HNPs is reasonable to result from the protonation of the piperazine units, which block the PET process from the methyl-substituted nitrogen atom to the NDI fluorophore [63].

Since NDI is a typical ICT chromophore, its fluorescence is critically dependent upon the solvent polarity. Therefore, to further investigate the validity of the encapsulation of NDI molecules in the

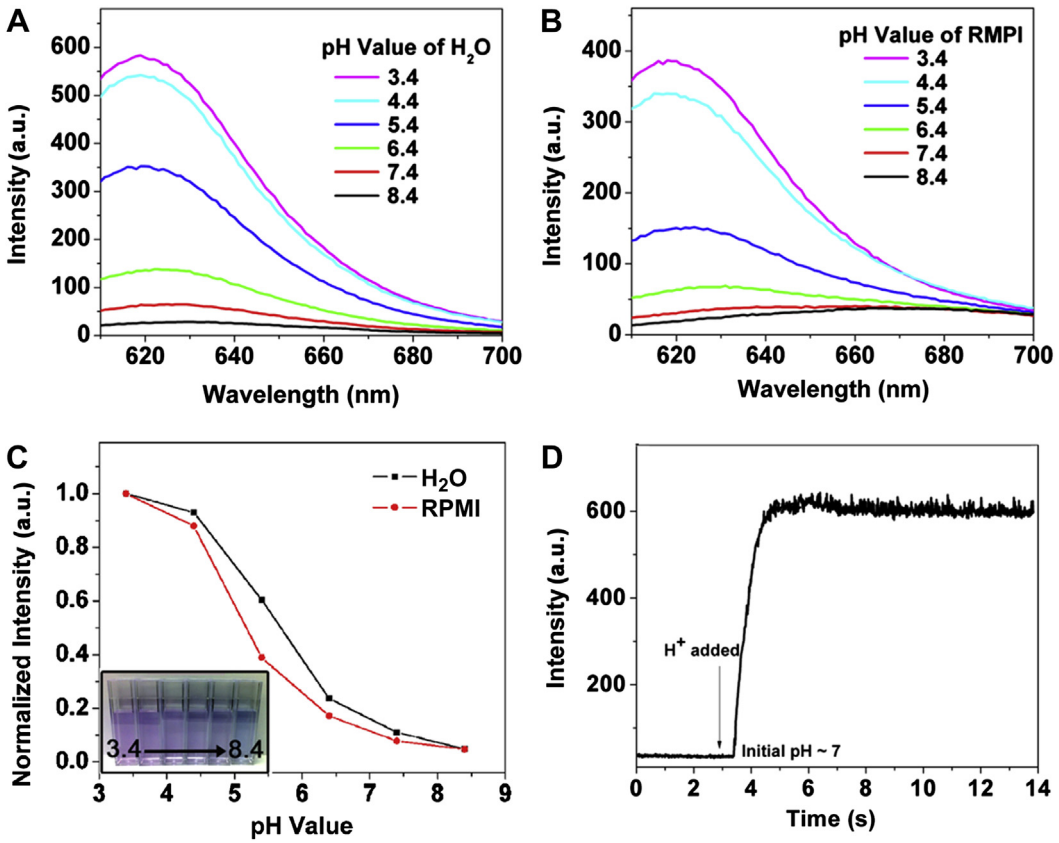

Fig. 3. pH-dependent fluorescence spectra of the as-synthesized NDI@HNPs in (A) H_2O and (B) cell culture medium RPMI ($\lambda_{ex} = 565$ nm). (C) Change in fluorescence intensity at 622 nm of NDI@HNPs in H_2O (black) and cell culture medium RPMI (red) as a function of pH value. Inset: photographic images of the as-synthesized NDI@HNPs in water under different pH. (D) Time dependence in fluorescent intensity at 622 nm of NDI@HNPs upon changing pH from 7 to 4 in water, data were recorded every 0.5 s. (For interpretation of the references to colour in this figure legend, the reader is referred to the web version of this article.)

Please cite this article in press as: Chang S, et al., A pH-responsive hybrid fluorescent nanoprober for real time cell labeling and endocytosis tracking, Biomaterials (2013), http://dx.doi.org/10.1016/j.biomaterials.2013.09.044

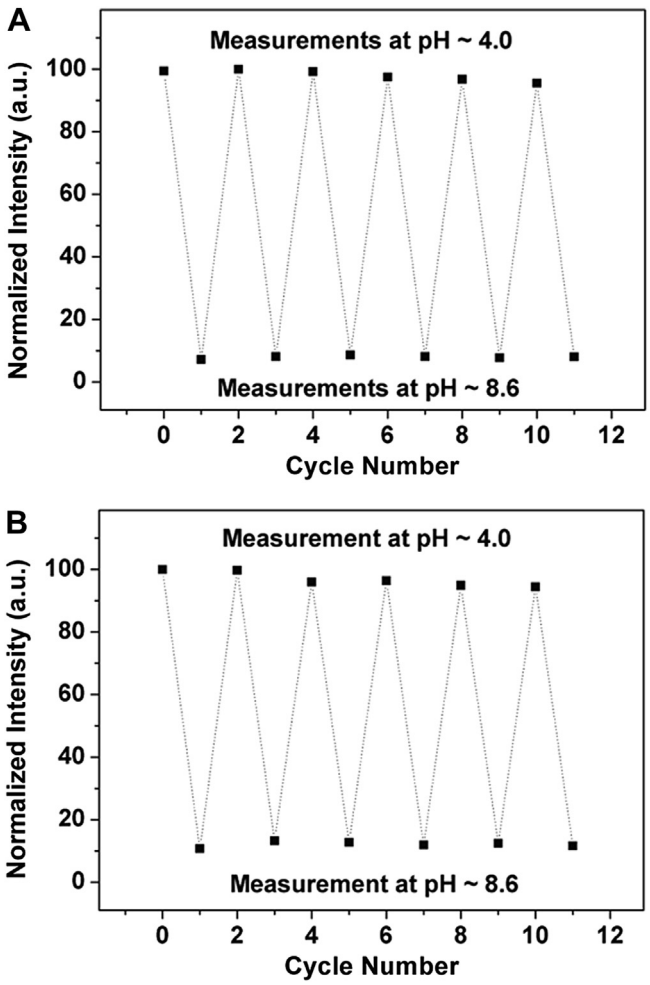

Fig. 4. Fatigue resistance of NDI@HNPs upon alternating pH changing from 4.0 to 8.6 (6 cycles) at room temperature: in water (A) and in phosphate buffered saline (PBS) solution.

nanospheres and the superiority brought by the encapsulation, the solvent effect on NDI fluorescence was studied. The solvent polarity was adjusted by using chloroform, acetone, DMF and DMF/H_2O mixture with different ratio. Unlike the complete water-solubility of NDI@HNPs brought by the high hydrophilicity of the outer shell layer, at least 5% DMF should be used in aqueous solution of NDI. As expected, along with the increasing polarity of solvents, the fluorescence enhancement ratio and fluorescence intensity in acidic medium simultaneously decrease dramatically, indicative of the serious and adverse impact of solvent polarity on fluorescence of NDI (Supporting Information: Table S1 and Fig. S7). Importantly, the difference between the aqueous solution of NDI (5% DMF) and NDI@HNPs exhibits that the encapsulation of NDI molecules into the weak polarity environment cavity can screen the effect of high polar solvents such as water. Accordingly, the encapsulation endows NDI@HNPs much better pH-response sensitivity and much stronger fluorescence intensity in acid environment (Fig. 2) even in pure aqueous system. Noticeably, the long emission wavelength at 622 nm makes NDI@HNPs a more promising pH-indicator for cell imaging with low scattering and minimal interfering fluorescence from biological system (Supporting Information: Table S1) [64,65].

To reveal the precise pH-dependence of the fluorescence intensity of NDI@HNPs, the fluorescence spectra of NDI@HNPs were recorded both in H_2O and cell culture RPMI mediums with different pH values (Fig. 3A and B), respectively. Upon changing pH from 8.4 to 3.4, the intensity of the emission peak at 622 nm increases gradually in pure aqueous solution with a final enlargement of about 55-fold in fluorescence intensity (calculated from Fig. 3C), accompanied with the gradual color change from blue to purple (Inset of Fig. 3C). Similar enhancement in fluorescence intensity was also observed in the case of the RPMI solution of NDI@HNPs (Fig. 3C). Additionally, the acidic constant (p*K*a) of NDI@HNPs in water was calculated to be *ca.* 5.61, based on the Henderson-Hasselbalch treatment [66]. It can be concluded that the typical PET process from the methyl-substituted nitrogen atom to the NDI fluorophore could be blocked by the protonation of the piperazine units stepwise during the gradual decrease of pH value. Clearly, in the pH range from 8.4 to 3.4, the excitonic emission of NDI@HNPs could be sufficiently manipulated by controlling the pH value of the mediums, which meets the physiological range for most live activities. This pH-responsive fluorescence property of NDI@HNPs could be applied in sensing the acidic endosomes by monitoring the alternation of the PL intensity. Moreover, all the sample solutions maintain transparent without any aggregation during testing processes, indicative of the long-time monodisperse property of NDI@HNPs at the various pH values. Furthermore, the pH response rate of NDI@HNPs with the environmental pH value was estimated by time-course fluorescence measurement of NDI@HNPs upon changing pH value in aqueous system. As shown in Fig. 3D, a sharp increase in fluorescence intensity at 622 nm of NDI@HNPs was observed in water solution once the pH value was changed, demonstrating that NDI@HNPs can respond promptly to the environmental pH change. It is suggestive that NDI@HNPs could be a potential candidate for real-time tumor imaging against physiologically pH conditions.

In the meantime, the fatigue resistance and reliability of the pH-triggered fluorescence intensity change of NDI@HNPs were measured in both water (Fig. 4A) and PBS (Fig. 4B) solution. After 6 cycles of reversible pH adjustments between 4.0 and 8.6, a slight drop of the fluorescence intensity at pH 4.0 was observed, while the fluorescence quenching state at pH 8.6 remained almost constant. These results in both water and PBS systems verify that NDI@HNPs possess a well reproducible pH-response fluorescence property, which probably benefits from the appropriate protection by cross-linked shell. It is thus proposed that such a system might be a satisfactory protocol for the intracellular pH detection and regulation of tumor models.

3.4. Tumor cell imaging, flow cytometry and in vitro cytotoxicity

Rapid cell-penetrating peptides (HIV-1 TAT) were conjugated onto the shells of HNPs (TAT-NDI@HNPs) through an amidation reaction to increase the cell-penetrating capability of NDI@HNPs. In order to further evaluate the labelinglabeling feasibility of TAT-NDI@HNPs on cell organelles, confocal laser scanning microscopy (CLSM) imaging as well as the flow cytometry analysis was conducted on human breast cancer cells (MCF-7) after co-cultivated with TAT-conjugated NDI@HNPs for different periods (Fig. 5). For the sake of convenient observation, the nuclei of MCF-7 were stained by Hoechst 33258 to emit blue fluorescence for live cells. Lysosomes were selectively stained with a green fluorescence by LysoTracker® Green-DND 99 (Invitrogen), a specific marker for these acidic organelles, while the dye-encapsulated nanoparticles TAT-NDI@HNPs were observed in red fluorescence under the sequential frame to prevent the interferences between different channels. The co-localization of the nanoparticles with specific organelle dyes was visualized in yellow fluorescence.

After co-cultivation for 1 h, almost no red fluorescence was detected in the cells. With the co-cultivation period prolonged to 4 h and especially 8 h, bright red spots were clearly observed from

Please cite this article in press as: Chang S, et al., A pH-responsive hybrid fluorescent nanoprober for real time cell labeling and endocytosis tracking, Biomaterials (2013), http://dx.doi.org/10.1016/j.biomaterials.2013.09.044

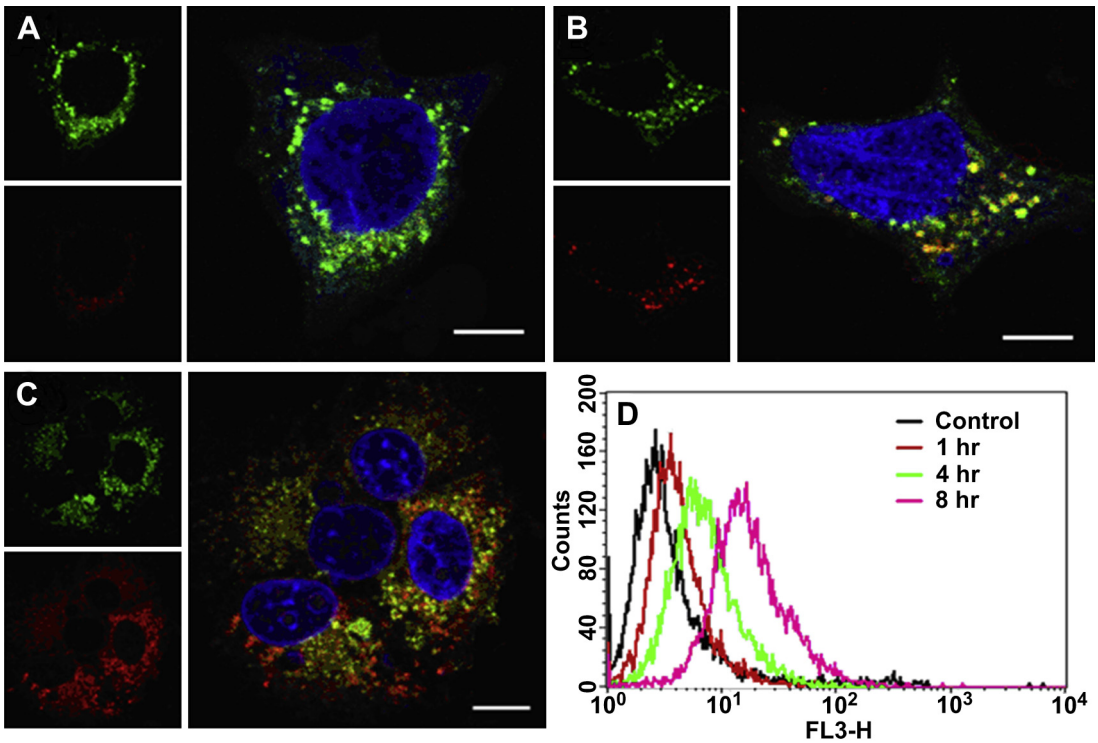

Fig. 5. Confocal laser scanning microscopic (CLSM) images of MCF-7 cells cultured at 37 °C with TAT-NDI@HNPs for (A) 1, (B) 4 and (C) 8 h. Red channel: TAT-NDI@HNPs, green channel: stained with LysoTracker® Green DND-99, cell nucleus stained with Hoechst 33258, scale bar: 10 μm. (D) Flow-cytometry analysis of MCF-7 cells incubated with TAT-NDI@HNPs for 1, 4 and 8 h. Untreated control cells were used as reference (black). (For interpretation of the references to colour in this figure legend, the reader is referred to the web version of this article.)

TAT-NDI@HNPs, perfectly matching with the green parts in the stained lysosome to yield yellow signals in the merged images. As expected, these bright yellow spots were mainly distributed in the acidic lysosomes environment. Obviously, TAT-NDI@HNPs were accumulated into the endolysomes of MCF-7 cells in 4 h co-cultivation, and TAT-NDI@HNPs were further assembled into the late endosome stage in 8 h co-cultivation, along with a bright red emission. When extending the co-cultivation time duration to 20 h (Supporting Information: Fig. S8), a large amount of TAT-NDI@HNPs were released into the cytoplasm so that the red fluorescence became decreased, and no longer overlaid with the green fluorescent signal of the lysosome tracker. In the flow cytometry analysis, similar results were obtained (Fig. 5A). Compared to the control sample, the fluorescence signal slightly increased in 1 h cell-incubation with TAT-NDI@HNPs. With the progress of phagocytosis, the fluorescence signal significantly increased in 4 h incubation, and yielded a stronger fluorescence signal in 8 h. This is also indicative of the significant accumulation of TAT-NDI@HNPs within the acidic organelles, in consistence with the CLSM results. Compared with the normal Human liver L-02 cells, the flow cytometry results exhibited no increase in fluorescence intensity even in 8 h co-cultivation (Supporting Information: Fig. S9). It is well known that the normal cells have less acidic intracellular environments than the cancer cells, and are not able to uptake via phagocytosis as a large amount of nanosized particles as tumor cells. Consequently, TAT-NDI@HNPs could easily penetrate into the cancer cells with an *in situ* rapid response to the intracellular acidic pH for the specific organelles. With the assistance of the pH-responsive TAT-NDI@HNPs, we could successfully detect the pH difference in the intracellular environments between cancer cells and normal cells.

The MTT method was utilized to investigate the potential cytotoxicity of NDI@HNPs against MCF-7 cells under the suspension concentrations of 63, 125, 250, 500 and 1000 μg mL^{-1} (Supporting Information: Fig. S10). After 24 h co-cultivation with NDI@HNPs, the survival rates of MCF-7 cells maintained at 99% under a high nanoparticle concentration of 250 μg mL^{-1}, and at 93% even under the extremely high concentration of 1000 μg mL^{-1}, indicative of negligible potential cytotoxicity of NDI@HNPs in the *in vitro* cell experiments. Since Hoechst 33258 can only stain living cells, the blue fluorescence signal from the CLSM images also proves the low cytotoxicity of NDI@HNPs.

From both the CLSM and flow cytometry studies, it is clear that these probes could permeate through the cytomembrane, along with intensified fluorescence signals to the acidic organelles in the cancer cells. The high cell penetration rate and the proton recognition can benefit the efficiently intracellular pH indication during the intracellular delivery. Such TAT-NDI@HNPs nanoprobes for optical cell-labelling would potentially facilitate the combined optical diagnosis in biomedical study and the cell response to drug delivery.

4. Conclusions

In summary, we have demonstrated a new robust strategy to develop highly sensitive intracellular pH-responsive fluorescent nano-hybrids for non-invasive cancer diagnosis and real time intracellular imaging. The facile immobilization of hydrophobic NDI fluorophores into the spherical PS-*b*-PAA micelles with shell cross-linking enables the resulting nanoprobes NDI@HNPs with a typical spherical morphology of 46 nm in diameter and excellent monodispersity in aqueous solutions. It is demonstrated that the NDI@HNPs nanoprobe possesses fast real-time pH response, extremely low cytotoxicity and enhanced turn-on fluorescence under acidic environment in highly polar aqueous systems with respect to the free NDI dye. The fluorescence intensity of NDI@HNPs

Please cite this article in press as: Chang S, et al., A pH-responsive hybrid fluorescent nanoprober for real time cell labeling and endocytosis tracking, Biomaterials (2013), http://dx.doi.org/10.1016/j.biomaterials.2013.09.044

is enhanced by 55-fold upon changing pH value from neutral (pH = 7.4) or basic (pH = 8.4) to acid (pH = 3.4) in pure aqueous system, in contrast to the serious fluorescence quenching of free NDI in the same medium. Together with the favorable wavelength of excitation (565 nm) and emission (622 nm), it can exactly meets the physiological pH range in cells, along with low scattering and minimal interfering requirements for fluorescent bioimaging. The prompt pH-responsive characteristics of NDI@HNPs endow the capability of intracellular labelling, organelle targeting, and the real time tracking of the probe entry into the cancer cells, the accumulation into the endolysosome and the further escape.

Acknowledgments

This work was financially supported by National 973 Program (2012CB933602, 2013CB733700), National Natural Science Foundation of China (51172070, 51132009, 51202068 and 61077085), the Oriental Scholarship, SRFDP 20120074110002, Program for New Century Excellent Talents in University (NCET-10-0379), Shuguang Project (11SG30), Scientific Innovation Project of Shanghai Municipal Education Commission (11ZZ53), Fundamental Research Funds for the Central Universities (222201313010, WD1114002, WD1124010 and WK1013002).

Appendix A. Supplementary data

Supplementary data related to this article can be found at http://dx.doi.org/10.1016/j.biomaterials.2013.09.044.

References

[1] Yuan L, Lin W, Zheng K, He L, Huang W. Far-red to near infrared ananlyte-responsive fluorescent probes based on organic fluorophore platforms for fluorescence imaging. Chem Soc Rev 2013;42:622–61.
[2] Tang R, Lee H, Achilefu S. Induction of pH sensitivity on the fluorescence lifetime of quantum dots by NIR fluorescent dyes. J Am Chem Soc 2012;134:4545–8.
[3] Liu Q, Yin B, Yang T, Yang Y, Shen Z, Yao P, et al. A general strategy for biocompatible, high-effective upconversion nanocapsules based on triplet-triplet annihilation. J Am Chem Soc 2013;135:5029–37.
[4] Liu Q, Yang T, Fang W, Li F. Blue-emissive upconversion nanoparticles for low-power-excited bioimaging in vivo. J Am Chem Soc 2012;134:5390–7.
[5] Guo Z, Song NR, Moon JH, Kim M, Jun EJ, Choi J, et al. A benzobisimidazolium-based fluorescent and colorimetric chemosensor for CO_2. J Am Chem Soc 2012;134:17846–9.
[6] Peng X, Yang Z, Wang J, Fan J, He Y, Song F, et al. Fluorescence ratiometry and fluorescence lifetime imaging: using a single molecular sensor for dual mode imaging of cellular viscosity.J. Am Chem Soc 2011;133:6626–35.
[7] Maxfield FR, McGraw TE. Endocytic recycling. Nat Rev Mol Cell Biol 2004;5:121–32.
[8] Izumi H, Torigoe T, Ishiguchi H, Uramoto H, Yoshida Y, Tanabe M, et al. Cellular pH regulators: potentially promising molecular targets for cancer chemotherapy. Cancer Treat Rev 2003;29:541–9.
[9] Nishi T, Forgac M. The vacuolar (H^+)-ATPases-nature's most versatile proton pumps. Nat Rev Mol Cell Biol 2002;3:94–103.
[10] Webb BA, Chimenti M, Jacobson MP, Barber DL. Dysregulated pH: a perfect storm for cancer progression. Nat Rev Cancer 2011;11:671–7.
[11] Kobayashi H, Ogawa M, Alford R, Choyke PL, Urano Y. New strategies for fluorescent probe design in medical diagnostic imaging. Chem Rev 2010;110:2620–40.
[12] Casey JR, Grinstein S, Orlowski J. Sensors and regulators of intracellular pH. Nat Rev Mol Cell Biol 2010;11:50–61.
[13] Yu H, Xiao Y, Jin L. A lysosome-targetable and two-photon fluorescent probe for monitoring endogenous and exogenous nitric oxide in living cells. J Am Chem Soc 2012;134:17486–9.
[14] Han J, Burgess K. Fluorescent indicators for intracellular pH. Chem Rev 2010;110:2709–28.
[15] Tantama M, Hung YP, Yellen G. Imaging intracellular pH in live cells with a genetically encoded red fluorescent protein sensor. J Am Chem Soc 2011;113:10034–7.
[16] Hu JM, Zhang XZ, Wang D, Hu XL, Liu T, Zhang GY, et al. Ultrasensitive ratiometric fluorescent pH and temperature probes constructed from dye-labeled thermoresponsive double hydrophilic block copolymers. J Mater Chem 2011;21:19030–8.
[17] Dennis AM, Rhee WJ, Sotto D, Dublin SN, Bao G. Quantum dots-fluorescent protein FRET probes for sensing intracellular pH. ACS Nano 2012;6:2917–24.
[18] Srikun D, Albers AE, Chang CJ. A dendrimer-based platform for simultaneous dual fluorescence imaging of hydrogen peroxide and pH gradients produced in living cells. Chem Sci 2011;2:1156–65.
[19] Benjaminsen RV, Sun HH, Henriksen JR, Christensen NM, Almdal K, Andresen TL. Evaluating nanoparticle sensor design for intracellular pH measurements. ACS Nano 2011;5:5864–73.
[20] Albertazzi L, Storti B, Marchetti L, Beltram F. Delivery and subcellular targeting of dendrimer-based fluorescent pH sensor in living cells. J Am Chem Soc 2010;132:18158–67.
[21] Urano Y, Asanuma D, Hama Y, Koyama Y, Barrett T, Kamiya M, et al. Selective molecular imaging of viable cancer cells with pH-activatable fluorescence probes. Nat Med 2009;15:104–9.
[22] Li C, Xia JA, Wei XB, Yan HH, Si Z, Ju SH. pH-activated near-infrared fluorescent nanoprobe imaging tumors by sensing the acidic microenvironment. Adv Funct Mater 2010;20:2222–30.
[23] Almutairi A, Guillaudeu SJ, Berezin MY, Achilefu S, Frechet JMJ. Biodegradable pH-sensing dendritic nanoprobes for near-infrared fluorescent lifetime and intensity imaging. J Am Chem Soc 2008;130:444–5.
[24] Jin P, Chu J, Miao Y, Tan J, Zhang S, Zhu W. A NIR luminescent copolymer based on platinum porphyrin as high permeable dissolved oxygen sensor for microbioreactor. AIChE J 2013;59:2743–52.
[25] Yin YD, Lu ZD. Colloidal nanoparticle clusters: functional materials by design. Chem Soc Rev 2012;41:6874–87.
[26] Yin YD, Liu YD, Goebl J. Templated synthesis of nanostructured materials. Chem Soc Rev 2013;42:2610–53.
[27] Li L, Choo ESG, Yi J, Ding J, Tang X, Xue J. Superparamagnetic silica composite nanospheres (SSCNs) with ultrahigh loading of iron nanoparticles via an oil-in DEG microemulsion route. Chem Mater 2008;20:6292–4.
[28] Kim J, Lee JE, Lee SH, Yu JH, Lee JH, Park TG, et al. Designed fabrication of a multifunctional polymer nanomedical platform for simultaneous cancer-targeted imaging and magnetically guided drug delivery. Adv Mater 2008;20:478–82.
[29] Lu Z, Gao C, Zhang Q, Chi M, Howe JY, Yin Y. Direct assembly of hydrophobic nanoparticles to multifunctional structures. Nano Lett 2011;11:3404–12.
[30] Lin Y, Boker A, Skaff H, Cookson D, Dinsmore AD, Emrick T, et al. Nanoparticle assembly at fluid interfaces: structure and dynamics. Langmuir 2005;21:191–4.
[31] Wu J, Yan Y, Liu B, Wang X, Li J, Yu J. Multifunctional open-framework zinc phosphate vertical bar $C_{12}H_{14}N_2$ vertical bar[Zn-6(PO_4)(4)(HPO_4)(H_2O)(2)]: photochromic, photoelectric and fluorescent properties. Chem Commun 2013;49:4995–7.
[32] Yang G, Wei Y, Xu S, Chen J, Li J, Liu Z, et al. Nanosize-enhanced lifetime of SAPO-34 catalysts in methanol-to-olefin reactions. J Phys Chem C 2013;117:8214–22.
[33] Taylor-Pashow KML, Della Rocca J, Huxford RC, Lin W. Hybrid nanomaterials for biomedical application. Chem Commun 2010;46:5832–49.
[34] Vollath D. Bifunctional nanocomposites with magnetic and luminescence properties. Adv Mater 2010;22:4410–5.
[35] Bardhan R, Lal S, Joshi A, Halas NJ. Theranostic nanoshells: from probe design to imaging ad treatment of cancer. Acc Chem Res 2011;44:936–46.
[36] Erathodiyil N, Ying JY. Functionalization of inorganic nanoparticles for bio-imaging applications. Acc Chem Res 2011;44:925–35.
[37] Lee JE, Lee N, Kim T, Kim J, Hyeon T. Multifunctional mesoporous silica nancomposite nanoparticles for theranostic application. Acc Chem Res 2011;44:893–902.
[38] Lu AH, Salabas EL, Schuth F. Magnetic nanoparticles: synthesis, protection, functionalization and application. Angew Chem Int Ed 2007;46:1222–44.
[39] Jun YW, Seo JW, Cheon J. Nanoscaling laws of magnetic nanoparticles and their aoolicabilities in biomedical sciences. Acc Chem Res 2008;41:179–89.
[40] Gao JH, Gu HW, Xu B. Multifunctional magnetic nanoparticles: design, synthesis and biomedical applications. Acc Chem Res 2009;42:1097–107.
[41] Wen S, Li XH, Ma HM. A tunable rationemtric pH senser based on carbon nanorods for the quantitative measurement of the intracellular oH of whole cells. Angew Chem Int Ed 2012;26:6538–41.
[42] Peng HS, Stolwijk JA, Sun LN, Wegener J, Wolfbeis OS. A nanogel for ratiometric fluorescent sensing of intracellular pH. Angew Chem 2010;122:4342–5.
[43] Rivera_Gil P, Nazarenus M, Ashraf S, Parak WJ. pH-sensitive capsules as intracellular optical reporters for monitoring lysosomal pH changes upon stimulation. Small 2012;8:943–8.
[44] Peng XJ, Song FL, Lu EH, Wang YN, Zhou W, Fan JL, et al. Heptamiethine cyanine dyes with a large Stokes shift and strong fluorescence: a paradigm for excited-state intramolecular charge transfer. J Am Chem Soc 2005;127:4170–1.
[45] He XX, Wang YH, Wang KM, Chen M, Chen SY. Fluorescence resonance energy transfer mediated large Stokes shifting near-infrared fluorescent silica nanoparticles for in vivo small-animal imaging. Anal Chem 2012;84:9056–64.
[46] Hotzer B, Medintz IL, Hildebrandt N. Fluorescence in nanobiotechnology: sophisticated fluorophores for novel applications. Small 2012;8:2297–326.
[47] Shcherbakova DM, Subach OM, Verkhusha VV. Red fluorescent proteins: advanced imaging applications and future design. Angew Chem Int Ed 2012;51:10724–38.
[48] Lu X, Zhu W, Shu Y, Li X, Gao Y, Li F, et al. Near-IR core-substitude naphthalenediimide fluorescent chemosensors for zinc ions: ligand effects on PET and ICT channels. Chem Eur J 2010;16:8355–64.

[49] Kang Y, Taton TA. Core/shell gold nanoparticles by self-assembly and cross-linking of micellar, block-copolymer shells. Angew Chem Int Ed 2005;44:409–12.
[50] Sakai N, Mareda J, Vauthey E, Matile S. Core-substitude naphthalenediimides. Chem Commun 2010;46:4225–37.
[51] Suraru S, Zschieschang U, Klauk H, Würthner F. A core-extended napthalene diimide as a p-channel semiconductor. Chem Commun 2011;47:11504–6.
[52] Shen LJ, Lu XY, Tian H, Zhu WH. A long wavelength fluorescent hydrophilic copolymer based on naphthalenediimide as pH sensor with broad linear response range. Macromolecules 2011;44:5612–8.
[53] Niu DC, Li YS, Qiao XL, Li L, Zhao WR, Chen HR, et al. A facile approach to fabricate functionalized superparamagnetic copolymer-silica nanocomposite spheres. Chem Commun 2008;37:4463–5.
[54] Chang S, Wu XM, Li YS, Niu DC, Ma Z, Zhao WR, et al. A hydrophobic dye-encapsulated nano-hybrid as an efficient fluorescent probe for living cell imaging. Adv Healthcare Mater 2012;1:475–9.
[55] Wu XM, Chang S, Sun XR, Guo ZQ, Li YS, Tang JB, et al. Construcitng NIR silica-cyanine hybrid nanocomposite for bioimaging in vivo: a breakthrough in photo-stability and bright fluorescence with large Stokes shift. Chem Sci 2013;4:1221–8.
[56] Owen SC, Chan DPY, Shoichet MS. Polymeric micelle stability. Nano Today 2012;7:53–65.
[57] Byrne JD, Betancourt T, Brannon-Peppas L. Active targeting schemes for nanoparticles systems in cancer therapeutics. Adv Drug Deliv Rev 2008;60:1615–26.
[58] Roger C, Miloslavina Y, Brunner D, Holzwarth AR, Würthner F. Self-assembled zinc chlorin rod antennae powered by peripheral light-harvesting chromophores. J Am Chem Soc 2008;130:5929–39.
[59] Oh E, Delehanty JB, Sapsford KE, Susumu K, Goswami R, Medintz IL, et al. Cellular uptake and fate of PEGylated gold nanoparticles is dependent on both cell-penetration peptides and particle size. ACS Nano 2011;5:6434–48.
[60] Albanese A, Chan WCW. Effect of gold nanoparticle aggregation on cell uptake and toxicity. ACS Nano 2011;5:5478–89.
[61] Huang WC, Chiang WH, Lin SJ, Lan YJ, Chen HL, Chern CS, et al. Lipid-containing polymer vesicles with pH/Ca^{2+}-ion-manipulated, size-selective permeability. Adv Funct Mater 2012;22:2267–75.
[62] He HR, Mortellaro MA, Leiner MJ, Young ST, Fraatz RT, Tusa JK. A fluorescent chemosensor for sodium based on photoinduced electron transfer. Anal Chem 2003;75:549.
[63] Myochin T, Kiyose K, Hanaoka K, Kojima H, Terai T, Nagano T. Rational design of ratiometric near-infrared fluorescent pH probes with various pKa values, based on aminocyanine. J Am Chem Soc 2011;133:3401–9.
[64] Benniston AC, Harriman A, Lawrie DJ, Mayeux A. The photophysical properties of a pyrene-thiophene-terpyridine conjugate and of its zinc(II) and ruthenium(II) complexes. Phys Chem Chem Phys 2004;6:51–7.
[65] Kaneda K, Arai T. Photoinduced hydrogen atom transfer in trans-1-(1′hydroxy-2′-naphthyl)-3-(1-napthyl)-2-propen-1-one. Photochem Photobiol Sci 2003;2:402–6.
[66] Bissell RA, Calle E, de Silva AP, de Silva SA, Gunaratne HQN, Habib-Jiwan JL, et al. Luminescence and charge transfer. Part 2. Aminomenthyl anthracene derivatives as fluorescent PET sensors for protons. J Chem Soc Perkin Trans 1992;2:1559–64.

Please cite this article in press as: Chang S, et al., A pH-responsive hybrid fluorescent nanoprober for real time cell labeling and endocytosis tracking, Biomaterials (2013), http://dx.doi.org/10.1016/j.biomaterials.2013.09.044